Available online at www.sciencedirect.com
SCIENCE DIRECT®
Journal of Solid State Chemistry 177 (2004) 3981–3986
JOURNAL OF SOLID STATE CHEMISTRY
www.elsevier.com/locate/jssc

Electrochemical performance of LiMSnO$_4$ (M = Fe, In) phases with ramsdellite structure as anodes for lithium batteries

M.V.V.M. Satya Kishore[a], U.V. Varadaraju[a,*], B. Raveau[b]

[a] *Materials Science Research Centre and Department of Chemistry, Indian Institute of Technology Madras, Chennai 600 036, Tamil Nadu, India*
[b] *Laboratoire CRISMAT, UMR 6508 CNRS, ENSICAEN, 6 Boulevard du Maréchal Juin, 14050, CAEN Cedex 4, France*

Received 26 April 2004; received in revised form 17 July 2004; accepted 20 July 2004
Available online 7 October 2004

Abstract

LiMSnO$_4$ (M = Fe, In) compounds were synthesized by high temperature solid-state reaction method and the electrochemical studies were carried out vs. lithium metal. Lithium is reversibly intercalated and deintercalated in LiFeSnO$_4$ with a constant capacity of ~90 mAh/g. In situ X-ray diffraction data show that ramsdellite structure is stable for lithium intercalation and deintercalation in LiFeSnO$_4$. Galvanostatic discharge/charge of LiFeSnO$_4$ in the voltage window 0.05–2.0 V shows a reversible capacity of ~100 mAh/g. The observed capacity in LiFeSnO$_4$ is due to the two processes involving alloying/dealloying of Li$_{4.4}$Sn and formation/decomposition of Li$_2$O. In contrast, the new isotypic oxide LiInSnO$_4$ does not exhibit any lithium intercalation due to the absence of mixed valence for indium. Its reversible capacity is strongly dependent on the voltage window. LiInSnO$_4$ exhibits severe capacity fading on cycling in the voltage window 0.05–2.0 V, but shows a stable capacity of ~90 mAh/g in the voltage range 0.75–2.0 V.

Keywords: Lithium batteries; Ramsdellite; Anode; Intercalation

1. Introduction

In commercial lithium-ion batteries, graphite is used as anode material and it has a theoretical specific capacity of 370 mAh/g. The demand to increase the energy density of lithium batteries has provoked the search for alternate anode materials with high capacity and good cyclability. Due to the high theoretical specific capacities of lithium metal alloys, several elements such as Sn, Si, and Al have been studied as anode materials [1,2]. Elemental tin shows high theoretical specific capacity of ~990 mAh/g corresponding to the formation of Li$_{4.4}$Sn alloy. However, the formation of Li$_{4.4}$Sn alloy during charge/discharge involves large volume changes. This causes cracking and crumbling of the electrode resulting in poor reversibility. Idota et al. [3] observed high capacity (~600 mAh/g) with good cyclability in amorphous tin composite oxide (ATCO). Courtney et al. [4] have shown that the lithium tin alloy is responsible for high capacity in ATCO and the mechanism of reaction of lithium with Sn based oxides was studied by in situ XRD. For example, in SnO$_2$ during initial discharge plateau Sn metal and Li$_2$O form followed by the formation of Li$_{4.4}$Sn alloy. The Li$_2$O formed in situ helps to minimize the effects of volume changes of Li$_{4.4}$Sn and thus the reversibility is enhanced in SnO$_2$ compared to Sn. But the main drawback of Sn based oxides is the large irreversible capacity loss in the first cycle due to the formation of inactive Li$_2$O.

Recently, Poizot et al. [5] demonstrated that simple transition metal oxides MO (M = Co, Ni, Fe and Cu) can react with lithium reversibly with capacities as high as 700 mAh/g. The reaction mechanism of lithium with MO involves the reversible formation and decomposition of Li$_2$O with concurrent reduction and oxidation of transition metal. The reversibility of transition metal oxides is strongly dependent on the voltage window,

*Corresponding author. +91-44-2257-0509.
E-mail address: varada@iitm.ac.in (U.V. Varadaraju).

0022-4596/$ - see front matter © 2004 Elsevier Inc. All rights reserved.
doi:10.1016/j.jssc.2004.07.026

particle size, cycling temperature and discharge rate. Recently, Obrovac et al. [6] proposed that the reaction of lithium with transition metal oxide like CoO, involves ion exchange process wherein the Co metal formed during discharge gets oxidized to Co^{2+} during charge and subsequently ion exchanges with Li^+ in Li_2O.

The presence of transition metal in tin based oxides may possibly reduce the irreversible capacity loss and also the presence of transition metal in the elemental state may possibly enhance the electronic conductivity of the matrix. In this perspective, Sn based compounds containing transition metal such as Co_2SnO_4 [7] and $NaFeSnO_4$ [8] have been studied as anode materials. It is interesting to note that in case of Co_2SnO_4 the cobalt metal formed during discharge is not oxidized during charge unlike in the case of CoO. In case of $NaFeSnO_4$, during charge, oxidation of iron metal is proposed for the capacity observed at high voltage.

In the present study, $LiMSnO_4$ ($M = Fe$, In) compounds with ramsdellite structure are evaluated as anode materials. $LiFeSnO_4$ has two polymorphs, a high temperature rasmdellite type structure and low temperature hexagonal close packed structure [9]. The ramsdellite structure is shown in Fig. 1. It consists of edge shared $(Fe,Sn)O_6$ octahedra forming rectangular tunnels . There are five possible sites in the tunnels, four tetrahedral (T_1, T_2, T_3, T_4) and one octahedral (O_c) site. Li^+ ions occupy these tunnels and distribute in two tetrahedral sites with preferential occupancy of the T_1 site [10]. Due to the presence of empty tetrahedral/octahedral sites, there is a feasibility of intercalation of lithium in $LiFeSnO_4$.

2. Experimental

The compounds $LiFeSnO_4$ and $LiInSnO_4$ were synthesized by high temperature solid state reaction method. The reactants were Li_2CO_3 (Merck, 99%), Fe_2O_3 (Merck, 99%), SnO_2 (Cerac, 99.9%) and In_2O_3 (Cerac, 99.9%). Appropriate amounts of reactants were ground well and heated at 600 °C for 12 h. The obtained products were ground and heated at 900 °C for 12 h, then at 1200 °C for 12 h followed by quenching at room temperature. An excess of 5 mol% Li_2CO_3 was added with respect to the ideal formula to compensate the loss of Li_2O at high temperature. Structural characterization of the compounds was done by powder X-ray diffraction (XRD) (Rich Seifert P3000, Germany, Co$K\alpha$ radiation). Unit cell parameters of the synthesized phases were calculated by using AUTOX program.

Electrodes for the electrochemical studies were prepared by mixing active material, acetylene black (Denka Singapore Pvt. Ltd) and poly-vinylidene fluoride in the weight ratios 70:20:10. The slurry prepared by using *n*-methyl-2-pyrrolidinone is spread on a stainless steel foil and dried in an oven at 100 °C for 12 h. Swagelok cells were fabricated in an argon filled glove box (mBraun, Germany, <5 ppm H_2O) with lithium metal as counter electrode, Teklon (Anatek, USA) as separator and 1 M $LiPF_6$ in 1:1 EC + DMC (Chiel Industries Ltd., Korea) as the electrolyte. Charge/discharge cycling of the cells were carried out in galvanostatic mode at room temperature by using Arbin battery cycling unit (BT 2000, USA).

In situ XRD measurements during lithium intercalation and deintercalation in $LiFeSnO_4$ were carried out by an in-house developed circular in situ XRD cell with beryllium window. $LiFeSnO_4$ with acetylene black and binder is directly deposited on the beryllium window and the cell was mounted on XRD machine (Rich Seifert, Co$K\alpha$ radiation) fitted with a secondary monochromator. During intercalation/deintercalation XRD patterns were taken in reflection mode at different Li contents.

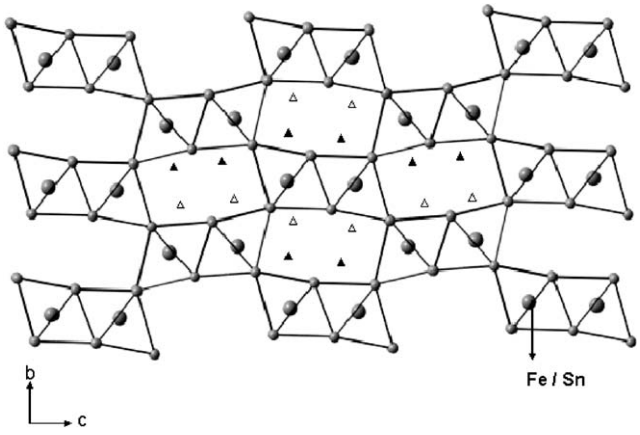

Fig. 1. Projection of the ramsdellite structure of $LiFeSnO_4$ along [100]. The partially occupied interstitial positions by lithium are shown as ▲ and △.

3. Results and discussion

3.1. $LiFeSnO_4$

3.1.1. Intercalation studies

The XRD pattern of $LiFeSnO_4$ is shown in Fig. 2(a). All the reflections are indexed on the basis of orthorhombic unit cell with space group Pmcn. The lattice parameters calculated by least-squares fitting are $a = 3.064(5)$ Å; $b = 5.056(8)$ Å and $c = 9.85(2)$ Å. These values are in good agreement with the literature report [9].

Li/$LiFeSnO_4$ cell is discharged initially to a capacity corresponding to one lithium (109 mAh/g) and further charge/discharge cycles were carried out in the voltage range 0.75–2.5 V at $C/10$ rate. The discharge and charge curves are shown in Fig. 3. During discharge the initial

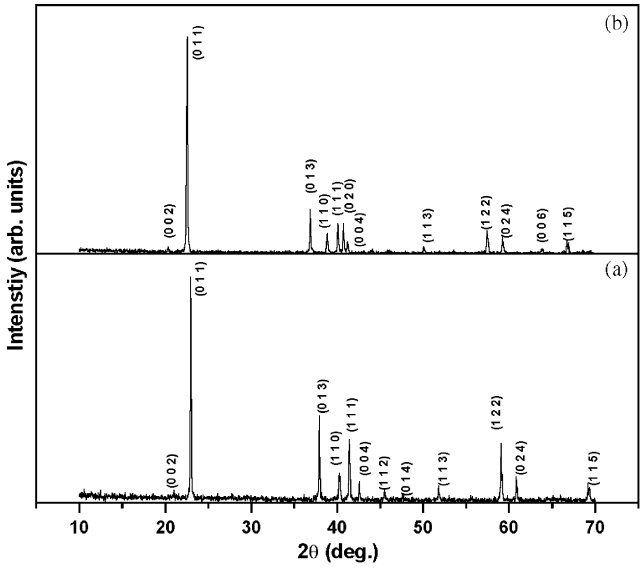

Fig. 2. Powder XRD patterns of (a) $LiFeSnO_4$ and (b) $LiInSnO_4$.

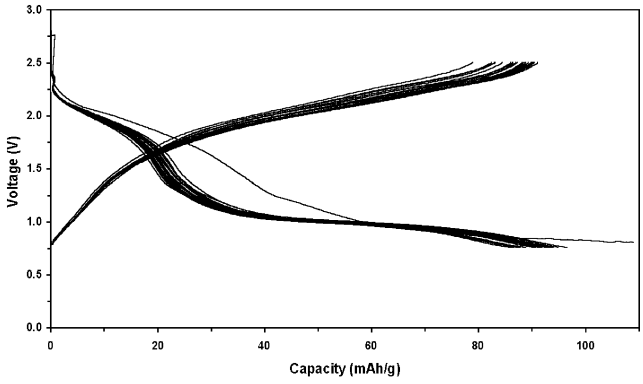

Fig. 3. Discharge and charge curves of Li/$LiFeSnO_4$ cell operated in the voltage range 0.75–2.5 V at $C/10$ rate.

small plateau at ~2.0 V (~0.2Li) can be attributed to the intercalation of Li into T_1 sites [10]. The second plateau at ~1.0 V can be attributed to the intercalation into T_2 sites. During charge the voltage increases smoothly to 2.5 V. A small hysteresis is observed during intercalation and deintercalation of lithium. This can be attributed to the changes in electronic conductivity of the intercalated phase compared to that of parent $LiFeSnO_4$ [11]. The redox couple that is responsible for the reversible lithium intercalation/deintercalation in $LiFeSnO_4$ is Fe^{3+}/Fe^{2+} [11]. The discharge capacity vs. cycle number of Li/$LiFeSnO_4$ in the voltage window 0.75–2.5 V is shown in Fig. 4. The second cycle discharge capacity is ~90 mAh/g and the value remains same even after 25 cycles.

The structural changes of $LiFeSnO_4$ during lithium intercalation and deintercalation are followed by in situ XRD. In situ XRD patterns during initial discharge/charge of lithium cell with $LiFeSnO_4$ as active material

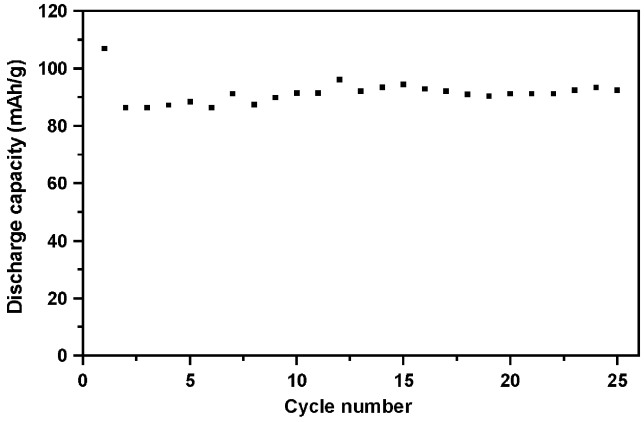

Fig. 4. Discharge capacity vs. cycle number of $LiFeSnO_4$ for the first 25 cycles in the voltage range 0.75–2.5 V.

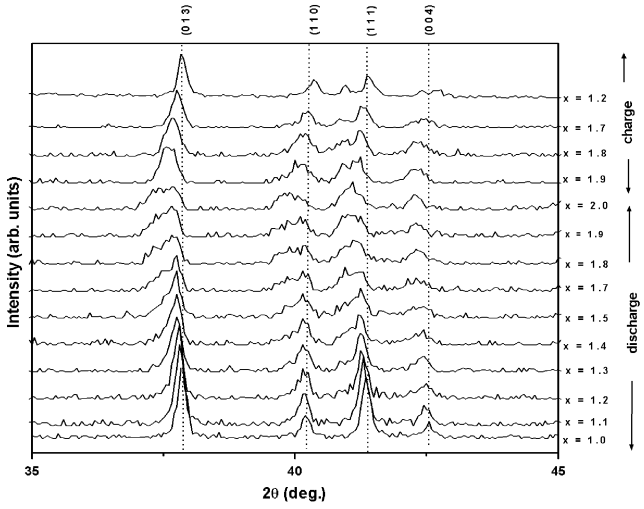

Fig. 5. In situ XRD patterns of Li_xFeSnO_4 at various Li contents during initial lithium intercalation and deintercalation.

are shown in Fig. 5. For clarity, the 2θ range 35–45° is shown. From the patterns it is evident that the structural integrity is maintained during the lithium intercalation/deintercalation process. There is no substantial change in the peak positions up to intercalation of 0.2Li. For intercalation of 0.3Li and above, peaks become broadened as expected for room temperature intercalation reactions. We observe peaks growing at lower 2θ corresponding to the intercalated phase. As the amount of lithium intercalated increases, the XRD patterns show that the parent phase progressively vanishes and the lithiated phase grows. The lattice parameters calculated for the end member Li_2FeSnO_4 phase are $a = 3.07(8)$ Å; $b = 5.12(5)$ Å and $c = 9.97(2)$ Å. The values are comparable to the values reported by

Greenblatt et al. [11]. During lithium deintercalation from Li_2FeSnO_4, XRD patterns show shift in the peak positions to higher angle and at the same time the intensities of the peaks also increases. The peak at $\sim 41^\circ$ in the XRD pattern of charged sample $Li_{1.2}FeSnO_4$ is due to the presence of small amount of Li_2FeSnO_4 phase. The peak positions of charged phase $Li_{1.2}FeSnO_4$ are same as that of original parent phase. This shows that although there is a structural dilation during intercalation in $LiFeSnO_4$ and the phase regains its original structure during deintercalation. The origin of good reversibility for lithium intercalation/deintercalation therefore can be attributed to the structural stability of $LiFeSnO_4$.

3.1.2. *$LiFeSnO_4$ as an anode material*

Voltage vs. capacity profiles of $LiFeSnO_4$ cycled in the voltage window 0.05–2.0 V at $C/5$ rate is shown in Fig. 6. During initial discharge a large plateau at 0.5 V is observed followed by a smooth curve to 0.05 V. The voltage behavior is different from that of SnO_2 wherein two steps are observed. It is reported in literature that the voltage plateau and behavior of Sn based oxides varies with counter cation and structure [12,13]. After subtracting the capacity due to acetylene black, the initial discharge capacity is 1175 mAh/g corresponding to reaction of $\sim$10.8Li. This large consumption of lithium indicates that as in the case of other Sn based oxides, the process involves destruction of the lattice to form $Li_{4.4}Sn$, Fe and Li_2O. The reaction can be written as follows:

$$LiFeSnO_4 + 11.4Li \rightarrow Li_{4.4}Sn + Fe + 4Li_2O. \quad (1)$$

The observed capacity value (10.8Li) is close to the theoretical value (11.4Li) confirming the occurrence of the above reaction. $LiFeSnO_4$ after initial discharge to 0.05 V is amorphous as evidenced by the ex situ XRD pattern and no reflections corresponding to parent phase are seen. This confirms that during discharge $LiFeSnO_4$ reacted completely. The cutoff voltage is fixed at 2.0 V for charge since there is a sharp increase in voltage above 2 V. During charge to 2.0 V, two steps are observed with a total capacity of 655 mAh/g, corresponding to extraction of $\sim$6Li. The charge capacity in the initial low voltage step (<1.0 V) can be attributed to the extraction of lithium from Li–Sn alloy. The report on FeO as anode material shows that Li_2O formed during initial discharge is decomposed in the voltage range 1.0–2.0 V [5]. Hence, the high voltage region of charge curve can be attributed to the re-oxidation of Fe to FeO associated with the decomposition of Li_2O. Thus the two processes that take place during charging can be written as:

$$Li_{4.4}Sn \rightarrow 4.4Li + Sn \quad (<1.0\,V), \quad (2)$$

$$Li_2O + Fe \rightarrow FeO + 2Li \quad (1.0 - 2.0\,V), \quad (3)$$

Due to the electrochemically active nature of Li_2O the faradaic efficiency of the first cycle observed for $LiFeSnO_4$ (58.3%) in the present study is greater than that of SnO_2 (39.5%).

On further cycling, the capacity observed is due to the reversibility of the above two processes (2) and (3). The discharge capacity vs. cycle number of $LiFeSnO_4$ cycled in the voltage window 0.05–2.0 V is shown in Fig. 7. Capacity corresponding to both the plateaus decreases with cycle number and the capacity reaches a stable value of $\sim$100 mAh/g after 25 cycles.

After the initial discharge to 0.05 V, $LiFeSnO_4$ is cycled in the voltage window 0.05–1.0 V. The initial charge capacity to 1.0 V is 245 mAh/g corresponding to extraction of $\sim$2.2Li. On cycling, the reversible capacity observed is due to alloying and dealloying of Li–Sn alloy in the matrix of Fe and Li_2O. The discharge capacity vs. cycle number (Fig. 7) shows that after first cycle, there is a marginal fade in capacity and the capacity ($\sim$150 mAh/g) is reasonably stable with cycle number.

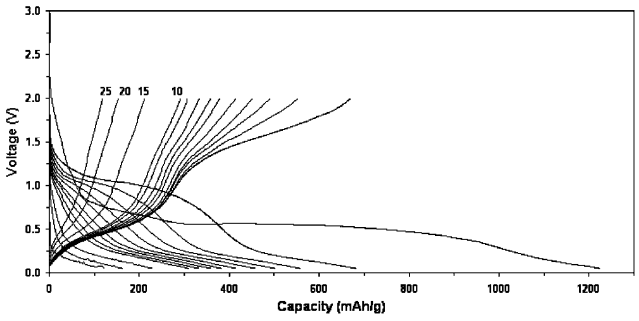

Fig. 6. Voltage vs. capacity profiles of $LiFeSnO_4$ cycled in the voltage window 0.05–2.0 V at $C/5$ rate.

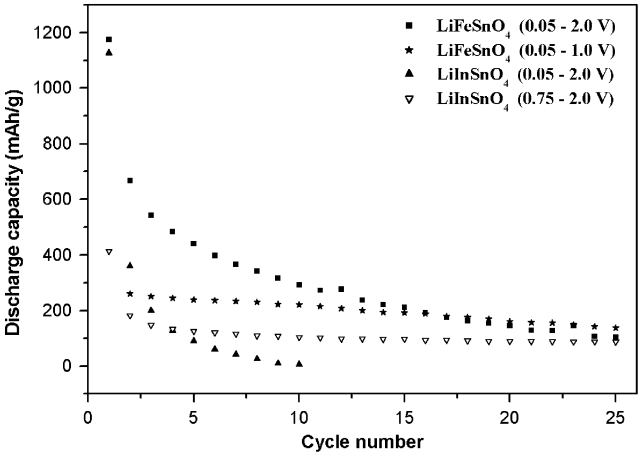

Fig. 7. Discharge capacity vs. cycle number of $LiFeSnO_4$ in the voltage windows 0.05–2.0 and 0.05–1.0 V and $LiInSnO_4$ in the voltage windows 0.05–2.0 and 0.75–2.0 V.

3.2. $LiInSnO_4$

In the present study, $LiInSnO_4$ which is isostructural with ramsdellite $LiFeSnO_4$ is synthesized for the first time. Our attempts to synthesize $LiMSnO_4$ compounds where M^{3+} = Al, Ga, Mn, Ni and Cr were not successful and the XRD patterns showed the major phase as SnO_2. The powder XRD pattern of $LiInSnO_4$ is shown in Fig. 2(b). All the reflections are indexed and the calculated lattice parameters are $a = 3.175(6)$ Å; $b = 5.130(8)$ Å; $c = 10.17(2)$ Å. There is an increase in all the cell parameters compared to $LiFeSnO_4$ due to the larger ionic size of In^{3+}. The XRD pattern of $LiInSnO_4$ heated to low temperature is similar to that of the ramsdellite phase, indicating that unlike in the case of $LiFeSnO_4$ there is no phase transition to the double hexagonal structure. Recently, indium based intermetallic compounds are shown to be promising anode materials for lithium batteries [14]. We have attempted to intercalate one lithium into $LiInSnO_4$. Even though a plateau is observed at ~1.0 V during discharge (intercalation) the charge capacity is negligible indicating no intercalation has taken place. This is further evident from the ex situ XRD studies (Fig. 8(a)), wherein there is a decrease in peak intensities without any change in the peak positions suggesting that the lithium reacts with the phase rather than intercalating into the structure. This shows that for intercalation to occur, a chemically reducible species such as Fe^{3+} which undergoes facile reduction in the operating voltage ranges is indeed necessary.

Voltage profiles of $LiInSnO_4$ initially discharged to 0.05 V and subsequent cycles up to 2.0 V at $C/5$ rate are shown in Fig. 9. The initial discharge curve shows a plateau at 1.0 V after an initial drop from OCV. After reaching a discharge capacity of 270 mAh/g, sloping profile with another plateau at ~0.5 V is observed followed by a smooth curve to 0.05 V. After correcting the capacity due to acetylene black, the initial discharge capacity of $LiInSnO_4$ is 1125 mAh/g. The initial charge curve shows smooth curve up to 0.8 V followed by a sharp rise in voltage to 2.0 V. Large irreversible capacity loss is observed on first cycle and the initial charge capacity is 375 mAh/g. Lithium can form various alloys Li_xIn ($1 \leqslant x \leqslant 3$); thus we can expect a maximum consumption of 14.4 lithium on initial discharge according to the following reaction:

$$LiInSnO_4 + 14.4Li \rightarrow Li_{4.4}Sn + Li_3In + 4Li_2O. \quad (4)$$

The observed capacity ~13Li indicates the formation of the various Li–In alloys. The ex situ XRD pattern (Fig. 8(c)) of $LiInSnO_4$ discharged to 0.05 V shows the formation of amorphous phases. Capacity faded significantly with cycle number and there is a negligible capacity value after 5 cycles (Fig. 7). The presence of In in the Sn–O matrix diminished the electrochemical performance of $LiInSnO_4$. The role of In is not clear, but similar observation is reported in case of In doped SnO_2, wherein capacity of 5% In_2O_3 doped SnO_2 faded significantly compared to SnO_2 [15].

To examine the effect of capacity retention on the voltage window, $LiInSnO_4$ cycled in the voltage window 0.75–2.0 V. The initial capacity up to 0.75 V corresponds to reaction of ~ 4.7Li. The ex situ XRD pattern (Fig. 8(b)) shows no reflections corresponding to parent $LiInSnO_4$ phase and the peak observed at 38.6° corresponds to In metal. Thus, the initial step can be attributed to the formation of In and simultaneous formation of several species such as Sn, SnO, SnO_2 and Li_2O. The cell cycled in the voltage window 0.75–2.0 V shows reversible extraction of lithium with a capacity of ~90 mAh/g (Fig. 7). The reversible capacity can be due

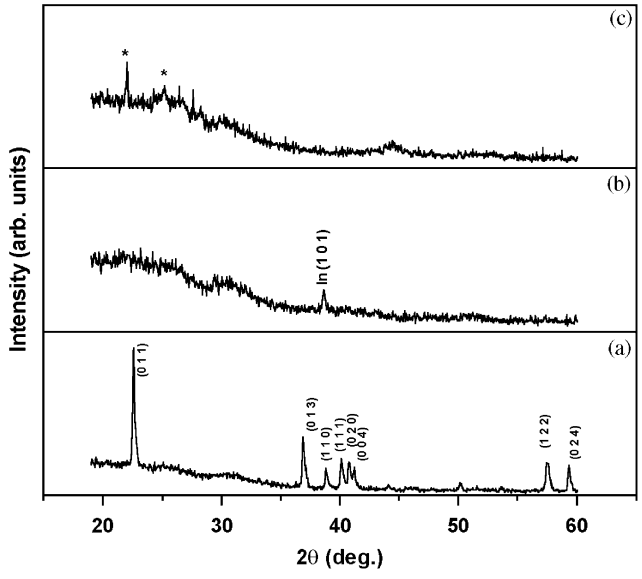

Fig. 8. XRD patterns of $LiInSnO_4$ electrode taken after (a) reaction of 1 Li (b) discharged to 0.75 V (c) discharged to 0.05 V. The asterisk (*) indicates separator peaks.

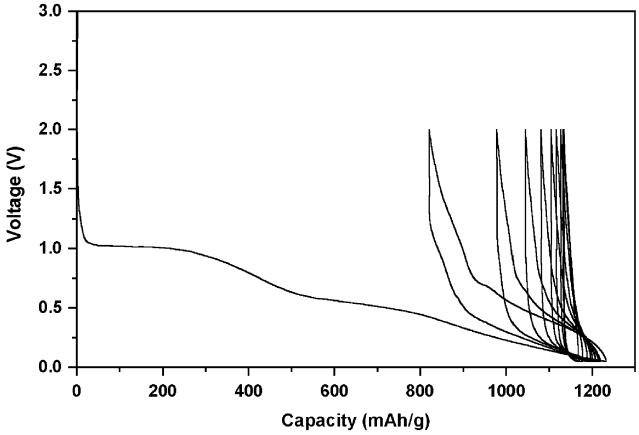

Fig. 9. Discharge and charge curves of $LiInSnO_4$ cycled in the voltage range 0.05–2.0 V at $C/5$ rate.

to the oxidation of Sn with the simultaneous decomposition of Li_2O [8].

4. Conclusions

During lithium intercalation and deintercalation in $LiFeSnO_4$, a reversible capacity of ~90 mAh/g is observed in the voltage range 0.75–2.5 V. The in situ XRD studies show that during lithium intercalation, structure undergoes dilation which is reversible on deintercalation. $LiFeSnO_4$ discharged to 0.05 V at $C/5$ rate leads to the formation of $Li_{4.4}Sn$, Li_2O and Fe. The Li_2O formed during initial discharge of $LiFeSnO_4$ is electrochemically active due to the presence of Fe. Thus, the irreversible capacity loss observed in $LiFeSnO_4$ for the first cycle is less compared to that of simple tin based oxides. $LiFeSnO_4$ displays a reversible capacity of ~100 mAh/g in the voltage range 0.05–2.0 V. A new compound $LiInSnO_4$ with ramsdellite structure has been synthesized and the voltage profile of $LiInSnO_4$ is qualitatively different compared to $LiFeSnO_4$. $LiInSnO_4$ cycled in the voltage window 0.05–2.0 V shows severe capacity fading, whereas good cycling performance (~90 mAh/g) is observed between 0.75 and 2.0 V. The low capacities obtained in these materials limit their use as anodes in lithium batteries.

References

[1] R.A. Huggins, J. Power Sources 81–82 (1999) 13–19.
[2] J.O. Besenhard, J. Yang, M. Winter, J. Power Sources 68 (1997) 87–90.
[3] Y. Idota, T. Kubota, A. Matsufuji, Y. Maekawa, T. Miyasaka, Science 276 (1997) 1395–1397.
[4] I.A. Courtney, J.R. Dahn, J. Electrochem. Soc. 144 (1997) 2045–2052.
[5] P. Poizot, S. Laruelle, S. Grugeon, L. Dupont, J.-M. Tarascon, Nature 407 (2000) 496–499.
[6] M.N. Obrovac, R.A. Dunlap, R.J. Sanderson, J.R. Dahn, J. Electrochem. Soc. 148 (2001) A576–A588.
[7] P.A. Connor, J.T.S. Irvine, Electrochim. Acta 47 (2002) 2885–2892.
[8] N. Sharma, K.M. Shaju, G.V. Subba Rao, B.V.R. Chowdari, J. Power Sources 124 (2003) 204–212.
[9] J. Choisnet, M. Hervieu, B. Raveau, P. Tarte, J. Solid State Chem. 40 (1981) 344–351.
[10] Ph. Lacorre, M. Hervieu, J. Pannetier, J. Choisnet, B. Raveau, J. Solid State Chem. 50 (1983) 196–203.
[11] M. Greenblatt, E. Wang, H. Eckert, N. Kimura, R.H. Herber, J.V. Waszczak, Inorg. Chem. 24 (1985) 1661–1665.
[12] M. Behm, J.T.S. Irvine, Electrochim. Acta 47 (2002) 1727–1738.
[13] P.A. Connor, J.T.S. Irvine, J. Power Sources 97–98 (2001) 223–225.
[14] J.T. Vaughey, J. O'Hara, M.M. Thackeray, Electrochem. Solid State Lett. 3 (2000) 13–16.
[15] J. Morales, L. Sánchez, Solid State Ionics 126 (1999) 219–226.